



HAL
open science

Effect of core-shell acrylate rubber particles on the thermomechanical and physical properties of biocomposites from polylactic acid and olive solid waste

Marwa Khemakhem, Khalid Lamnawar, Abderrahim Maazouz, Mohamed Jaziri

► To cite this version:

Marwa Khemakhem, Khalid Lamnawar, Abderrahim Maazouz, Mohamed Jaziri. Effect of core-shell acrylate rubber particles on the thermomechanical and physical properties of biocomposites from polylactic acid and olive solid waste. *Polymer Engineering and Science*, 2018, 58 (6), pp.894-902. 10.1002/pen.24642 . hal-01822759

HAL Id: hal-01822759

<https://hal.science/hal-01822759>

Submitted on 20 Feb 2023

HAL is a multi-disciplinary open access archive for the deposit and dissemination of scientific research documents, whether they are published or not. The documents may come from teaching and research institutions in France or abroad, or from public or private research centers.

L'archive ouverte pluridisciplinaire **HAL**, est destinée au dépôt et à la diffusion de documents scientifiques de niveau recherche, publiés ou non, émanant des établissements d'enseignement et de recherche français ou étrangers, des laboratoires publics ou privés.



Distributed under a Creative Commons Attribution - NonCommercial 4.0 International License

Effect of Core–Shell Acrylate Rubber Particles on the Thermomechanical and Physical Properties of Biocomposites from Polylactic Acid and Olive Solid Waste

Marwa Khemakhem ^{1,2,3}, Khalid Lamnawar,^{2,3} Abderrahim Maazouz,^{2,3,4} Mohamed Jaziri¹

¹ *Laboratoire Electrochimie et Environnement, ENIS, Université de Sfax, 3038 Sfax, Tunisie*

² *UMR 5223, Ingénierie des Matériaux Polymères IMP, CNRS, INSA Lyon, Villeurbanne 69621, France*

³ *Université de Lyon, INSA-LYON, Lyon 69361, France*

⁴ *Hassan II Academy of Science and Technology, 10 100 Rabat, Morocco*

Biocomposites from polylactic acid (PLA) and olive solid waste (OSW) were melt-blended with core–shell acrylate rubber particles (ACR) in order to enhance the thermal stability upon melt processing and the mechanical performances of these biocomposites, thereby expanding their area of application. Dynamic mechanical analysis indicated that the ACR particles imparted more flexibility to the PLA/OSW biocomposites and thermal analysis showed that the incorporation of ACR significantly restrained the ability of the PLA chains to crystallize. The values of complex viscosity and storage modulus were significantly increased with the introduction of ACR. These results could be assigned to the entanglements between the PLA chains and those of the ACR shell, giving rise to a physical network that limited the segmental mobility of PLA and induced a high melt elasticity. Mechanical tests revealed that the elongation at break and the impact strength of the biocomposites were considerably improved. Moreover, morphological observations showed a clear adhesion enhancement between the PLA matrix and the OSW fillers in the presence of the ACR additive.

INTRODUCTION

The current policies related to polymer materials are based on three principles: respecting the environment, reducing waste and pollutants and replacing materials derived from petroleum by renewable and sufficiently available materials [1]. In the polymer composites field, the substitution of synthetic fillers with natural ones is a current research topic for many economic, environmental and marketing reasons [2]. Actually, with the growing focus on environmentally friendly products, natural fillers have gained increasing interest from both academic and industrial communities. The main advantages of natural fillers, compared to their synthetic counterparts, are a low density, low cost, good thermal insulation, sustainability, and problem-free disposal [3]. They are neutral when it comes to CO₂ emissions to the atmosphere and require little energy to be produced.

Numerous researchers have taken interest in conventional polymer matrices, mostly polyolefins, in combination with

natural fibers and organic waste materials, such as rice husk ash, wood flour, and sawdust, among others [4–6]. However, these kinds of composites are not fully biodegradable, wherefore their eco-friendly performance is relatively low. To overcome this drawback, an innovative alternative would be to replace the traditional nonbiodegradable polymer matrices by biodegradable ones. Among the biodegradable polymers that are currently commercialized, poly(lactic acid) is of great interest for research since it can be prepared from annually renewable resources such as corn starch rather than oil or natural gas feedstocks.

PLA is a linear, aliphatic, and thermoplastic polyester that can be synthesized by direct condensation of lactic acid, which is produced from the fermentation of starch or sugar [7]. It displays some physical and mechanical properties comparable to those of many petroleum-derived polymers such as a high modulus, transparency and aroma barrier capabilities [8, 9]. PLA has become a potential candidate for various industrial applications, for instance in the biomedical, packaging and textile fields [10]. However, some major disadvantages include a high cost, low thermal stability and inherent brittleness, which might limit its use for large-scale applications [11]. These drawbacks can be roughly overcome by plasticization [12], copolymerization [13], and blending with other polymers or fillers [14].

In a recent study [15], biocomposites made from polylactic acid (PLA) and olive solid waste (OSW) were developed, with the aim to minimize fabrication costs and reduce waste from the olive oil industry. It was demonstrated that the OSW inclusion under high temperatures resulted in a degradation of the PLA matrix. Therefore, a chain extender agent named Joncryl and containing nine glycidyl methacrylate (GMA) functions was added to the biocomposites so as to enhance the thermal stability upon melt processing. However, a study of the mechanical properties showed that the designed biocomposites remained brittle even in the presence of Joncryl. The inherent fragility of the biocomposites induced a difficulty with regard to processability, which limited the number of possible applications. Based on these previous results, the next step was to amend this behavior.

Core–shell-type copolymers have been used to toughen brittle materials, such as epoxy products [16], polyvinyl chloride [17], and polycarbonate [18]. Recently, acrylic core–shell particles have been employed to obtain an effective method for PLA toughening. For example, Zhang et al. [19] blended PLA with 5–25 wt% of methyl methacrylate butadiene styrene (MBS). By increasing the MBS content, the tensile strength of the blends decreased; however, the elongation at break and impact strength were found to significantly increase. Sun et al. [20] introduced epoxy-functionalized grafted acrylonitrile butadiene styrene

Correspondence to: M. Khemakhem; e-mail: khemakhem.marwa1@gmail.com, K. Lamnawar; e-mail: khalid.lamnawar@insa-lyon.fr, A. Maazouz; e-mail: abderrahim.maazouz@insa-lyon.fr

TABLE 1. Composition of the prepared blends.

Sample name	Wt% of neat PLA in the blend	Wt% of OSW in the blend	Wt% of ACR in the blend
PLA	100	0	0
PLA/OSW (80/20)	80	20	0
PLA/OSW/ACR (77.5/20/2.5)	77.5	20	2.5
PLA/OSW/ACR (75/20/5)	75	20	5
PLA/OSW/ACR (70/20/10)	70	20	10

particles into the PLA matrix. A notched impact strength of 540 J/m was reached for the PLA/ABS-g-GMA blend with 1 wt% GMA, which was 27 times higher than the impact strength of pure PLA. Hao et al. [21] blended PLA with glycidyl methacrylate-functionalized methyl methacrylate butadiene (MB-g-GMA) copolymer. They noted a large plastic deformation in the blends when subjected to impact tests, which revealed an important energy-dissipation process and induced a toughened polymer. Acrylate copolymers (ACR) have also been used as a very effective impact modifier for PLA [22, 23].

ACR is a core-shell-type copolymer that consists of a rubbery poly(butyl acrylate) core encapsulated within a poly(methyl methacrylate) shell. The PBA inside the particle represents the soft phase that generates toughening while the thermoplastic glassy shell PMMA provides rigidity and allows a good dispersion of the rubber particles in the PLA matrix. In fact, PMMA is expected to entangle with the PLA molecules during processing given that PLA and PMMA have similar solubility parameters [24].

This article tried to provide a comprehensive study of the effects of small amounts of acrylic core-shell rubber particles on the physical, rheological, morphological, and thermomechanical properties of the biocomposites based on PLA matrix and OSW filler. To the best of our knowledge, no paper was published covering the whole of these topics. Some investigations have focused only on studying the thermal stability and mechanical performances of composites from polylactic acid and acrylates with or without adding natural fillers [25–27]. High amounts of acrylates (up to 25 wt%) were however used and no shear rheological effects were clearly discussed in correlation to their processing. Since a higher amount of these acrylates is used, the biodegradability of the composites is not guaranteed any longer. However, in the present study, low concentrations of ACR (2.5, 5, and 10 wt%) were added to the PLA/OSW biocomposites in order to improve the thermomechanical and the physical properties of these biocomposites while maintaining their biodegradable character. The main objective was to achieve a compromise between reducing the fabrication cost (by adding OSW), obtaining satisfactory properties (by adding ACR) and preserving the biodegradability of these composites.

EXPERIMENTAL

Materials

Poly(lactic acid, PLA2003D, was supplied by Natureworks. This grade corresponds to a semicrystalline polymer containing 4.3% of D-LA units.

Acrylic core-shell rubber (ACR) was purchased from Rohm and Haas Company as an Impact modifier, with a trade name of EXL 2330. Its density is between 0.41 and 0.57 g/cc. The average size of ACR nanoparticle is 250 nm, and the thickness of the shell PMMA layer is about 6 nm. The PBA/PMMA weight ratio is 86/14 (wt/wt). The core-shell-type copolymer used in this study is a versatile product consisting of a poly(butyl acrylate) core which improves impact properties due to its elastomeric nature and a poly(methyl methacrylate) shell which imparts a certain thermal resistance. Thus, the product is suitable for extrusion and compression processing conditions.

Olive solid waste is an industrial by-product provided by SISI, Tunisia. The oil extraction process generates large amounts of solid residues. After eliminating water, the solid residue is treated with hexane to recover the remaining oil. The hard stone is separated from the soft skin and then dried and ground into fine particles.

Preparation of Biocomposites

Before compounding, the PLA pellets, OSW, and ACR were dried in a vacuum oven at 80°C for 24 h to remove moisture. PLA biocomposites containing 20 wt% of OSW with and without ACR were prepared using a corotating twin-screw extruder (Thermo Electron Polylab System Rhecord RC400P) with a screw diameter of 16 mm and an L/D ratio of 25:1. The mixing was performed using a sealed hopper under a nitrogen atmosphere to avoid thermo-oxidative degradation and hydrolysis. The rotation speed was fixed at 40 rpm and the residence time in the extruder was about 2 min. The temperature profile along the extruder was set to 165°C (feeding zone), 190°C, 190°C, 170°C (melting zones), and 170°C (die). The composition of the prepared blends is given in Table 1.

After melt blending, the extrudates were cooled in a long water bath and granulated. The obtained granules were then compression-molded into disks for rheological characterization and into dumbbell-shaped specimens for mechanical testing.

Characterization

Dynamic Mechanical Analysis (DMA). DMA tests were performed using a Q800 DMA from TA instrument. Compression molded samples having a rectangular shape (14 mm × 7 mm × 1 mm) were used. The experiments were achieved in tension mode, with a constant heating of 3°C/min, a frequency of 1 Hz and a strain amplitude of 0.05%. The temperature range was from −70 to 140°C.

In order to obtain more accurate results, an annealing treatment was performed at 90°C during 3 h. Thus, the polymorphic nature of PLA could be overcome by deleting the cold crystallization of the polymer. DMA tests were conducted on the samples before and after being annealed.

Small Amplitude Oscillatory Shear Experiments (SAOS). The measurements were performed using a DHR-2 stress-controlled rotational rheometer from TA instruments. The dynamic frequency sweep tests were performed at 180°C under a nitrogen flow using a 25-mm parallel plate geometry and a gap of about 0.8 mm. Before the dynamic frequency sweep measurements, the linear domain was determined at a frequency of 0.1 rad/s and was found to range from 0.2 to 1,000 Pa. The stress

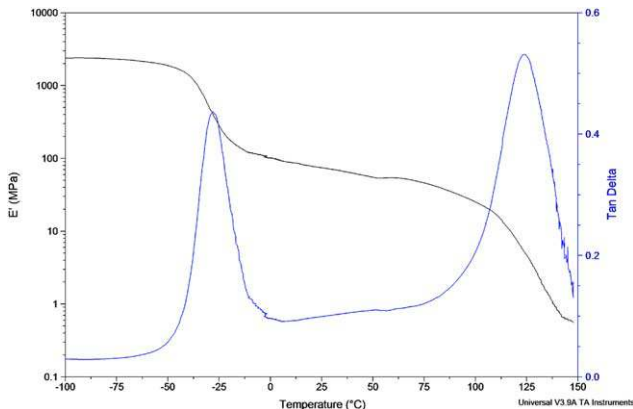


FIG. 1. Evolution of the storage modulus (E') and loss factor ($\tan \delta$) versus temperature for the acrylic core-shell rubber. [Color figure can be viewed at wileyonlinelibrary.com]

amplitude was fixed at 20 Pa to obtain reasonable signal intensities and the experiments were performed under a frequency range of 0.1–628 rad/s.

Differential Scanning Calorimetry (DSC). The thermal properties of neat PLA, the PLA/OSW biocomposites and the PLA/OSW/ACR blends were examined with the aid of a DSC Q20 differential scanning calorimeter from TA Instruments fitted with a liquid nitrogen cooling system (LNCS). Several heating/cooling cycles were performed under a nitrogen flow of 50 mL/min. The samples were first heated to 170°C and maintained at this temperature for 3 min to remove the material's thermal history. Subsequently, they were cooled down to -80°C at a cooling rate of 10°C/min. Finally, the samples were reheated to 170°C at 10°C/min. The percentage of crystallinity was calculated according to the following equation:

$$\chi_c(\%) = \frac{1}{f} \times \frac{\Delta H_m - \Delta H_\infty}{\Delta H_m^\infty} \times 100. \quad (1)$$

where ΔH_m and ΔH_m^∞ represent, respectively, the measured melting heat of the considered PLA and the fusion enthalpy of the completely crystalline PLA (93 J/g). The DSC measurements were conducted on the samples before and after annealing.

Mechanical Properties. Tensile tests were performed at room temperature (25°C) using an Instron testing machine. The dumb-bell specimen dimensions were 30 mm in length, 5 mm in width, and 2 mm in thickness. All samples were dried under vacuum for 3 h at 60°C before being tested at a crosshead speed of 5 mm/min.

Impact testing was carried out in accordance with the ISO 179-1/1 e A standard on a Charpy CEAST lot EP 3080 machine. The span length was 62 mm and the impact energy was 5 J. The specimens (80 mm × 10 mm × 4 mm) were notched at an angle of 45° and a depth of 2 mm. The impact strength value (kJ/m²) was calculated by dividing the obtained absorbed impact energy by the cross-section area of the samples. All reported values are averages of five experimental results for tensile and impact tests in order to verify reproducibility.

Scanning Electron Microscopy (SEM). The morphology of the fracture surface of the samples was observed by a scanning electron microscope (SEM; Hitachi S3500) under an accelerating voltage of 8 kV. The specimens were fractured at the temperature of liquid nitrogen after which the fracture surface was coated with gold for 60 s at an amperage value of 40 mA prior to observation.

RESULTS AND DISCUSSION

Solid State Viscoelastic Properties

The evolution of the storage modulus (E') and the loss factor ($\tan \delta$) as functions of temperature are presented in Fig. 1. This figure reveals the nature of the two phases (rubber and thermo-plastic) of the core-shell type copolymer. The mechanical relaxation temperatures associated with the glass transitions of both phases, respectively at -45 and 115°C, affirm that the elastomeric phase inside the core-shell particle was poly(butyl acrylate), whereas the thermoplastic phase constituting the hard coating was poly(methyl methacrylate) [28].

Figure 2 shows the obtained results in terms of the real part of the dynamic complex modulus (E') and the loss factor ($\tan \delta$) for neat PLA and the biocomposites incorporating 20 wt% of OSW and containing different amounts of acrylate copolymer (0, 2.5, 5, and 10 wt%).

For the studied systems, the mechanical relaxation peaks ($\tan \delta$ curve) associated with the glass transition (E' curve) of the three main components of the material can be distinguished as follows:

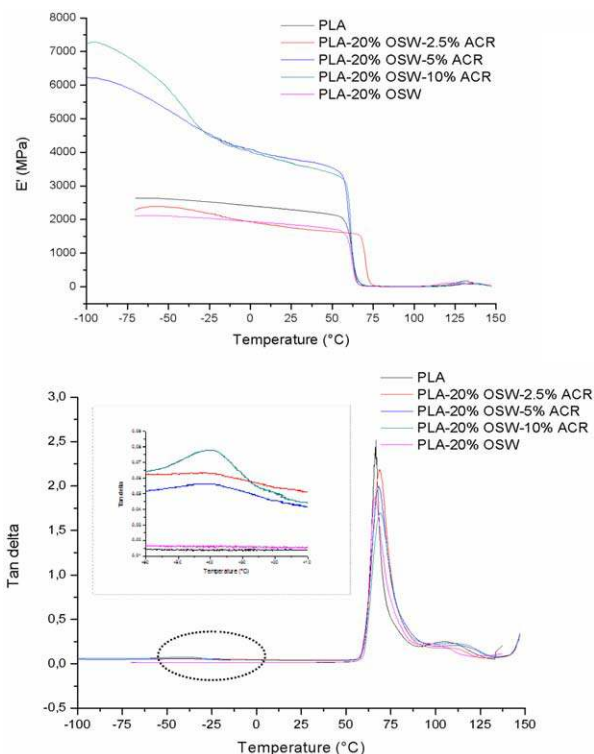


FIG. 2. Storage modulus (a) and loss factor (b) as a function of temperature for neat PLA and PLA-20 wt% OSW biocomposites with various amounts of ACR (0, 2.5, 5, and 10 wt%). [Color figure can be viewed at wileyonlinelibrary.com]

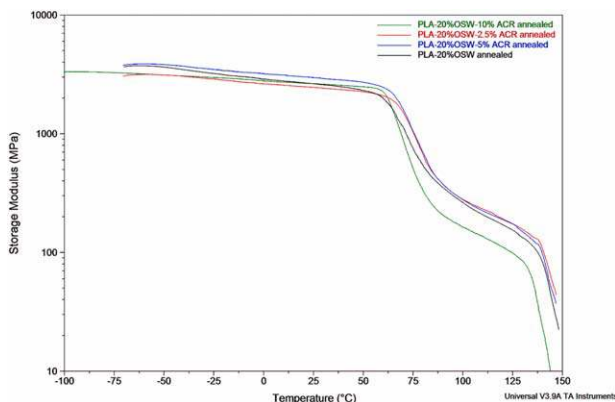


FIG. 3. Storage modulus versus temperature for annealed (PLA/OSW) (80/20) biocomposites containing different amounts of ACR. [Color figure can be viewed at wileyonlinelibrary.com]

- In the low temperatures range, at around -40°C , a relaxation peak of very low amplitude was detected for the biocomposites containing ACR. It was attributed to the glass transition of the elastomeric phase, poly (butyl acrylate), established within the core-shell dispersed nodules.
- At higher temperatures ($60\text{--}90^{\circ}\text{C}$), the pure PLA and the PLA/OSW biocomposite show a single peak (62.8°C) attributed to the glass transition. The biocomposites containing ACR particles exhibit a single high temperature peak between that of pure PLA and that of PMMA. It corresponds to the relaxations associated with the concomitant glass transitions of the PLA matrix and the PMMA shell. This result revealed that the PLA was partially miscible with PMMA. Miscibility between PLA and the shell component is very important for achieving good ultimate mechanical properties, because it enhances the interfacial adhesion phase. Moreover, the peak height of the biocomposites containing ACR gradually decreased compared to that of pure PLA. This could be explained by the gradually increased flexibility of these biocomposites.
- In the high temperature range ($90\text{--}125^{\circ}\text{C}$), a low intensity broad relaxation peak was identified. This transition appeared for the neat PLA as well as the prepared blends and may be attributed to the cold crystallization of the PLA matrix.

In order to confirm the obtained results, the annealed samples were tested. In fact, the annealing treatment enabled the removal of the PLA cold crystallization. Therefore, it would be easier to compare the rubbery moduli of the different compositions in the temperature range of $90\text{--}125^{\circ}\text{C}$.

Figure 3 illustrates the results obtained after annealing in terms of storage modulus (E') for the PLA-20 wt% OSW biocomposites with different ACR contents. It is clear that the rubbery modulus significantly declined after addition of the core-shell particles to the composite system. In fact, at 100°C , its value decreased from 300 MPa for PLA-20 wt% OSW biocomposite to 153 MPa for the composite containing 10 wt% of ACR. This result indicates the ability of the core-shell particles to impart a greater flexibility to the material. Similar results were found by Liang et al. [29]. This behavior would affect the mechanical properties by giving rise to a greater elasticity for small deformations and a better ductility for high deformations.

Shear Melt Rheology

The evolution of the rheological properties in the molten state as a function of frequency was investigated. Figure 4 displays the results of the viscoelastic tests obtained in dynamic mode at 180°C for neat PLA and the biocomposites containing 20 wt% of OSW with various core-shell particle contents (0, 2.5, 5, and 10 wt%).

The complex viscosity modulus of the PLA-20% OSW biocomposite was lower than that of the neat PLA. In fact, the presence of hydroxyl groups in the hydrophilic OSW filler favored alcoholysis or hydrolysis of the PLA matrix, which could be responsible for the higher losses of molar masses in the PLA/OSW biocomposites compared with the neat PLA [15]. However, the incorporation of ACR into the PLA/OSW biocomposite significantly raised the viscosity with increasing core-shell particle content (Fig. 4a). This could be due to the establishment of a network of molecular entanglements between the PLA and PMMA chains enveloping the dispersed core-shell (CS) particles. The formed interphase thus improved the adhesion between the components and enhanced the anchoring of the core-shell particles [30]. In fact, the acrylic copolymer present in the system resulted in the intermingling of the PLA and PMMA chains through their proven miscibility. The density of

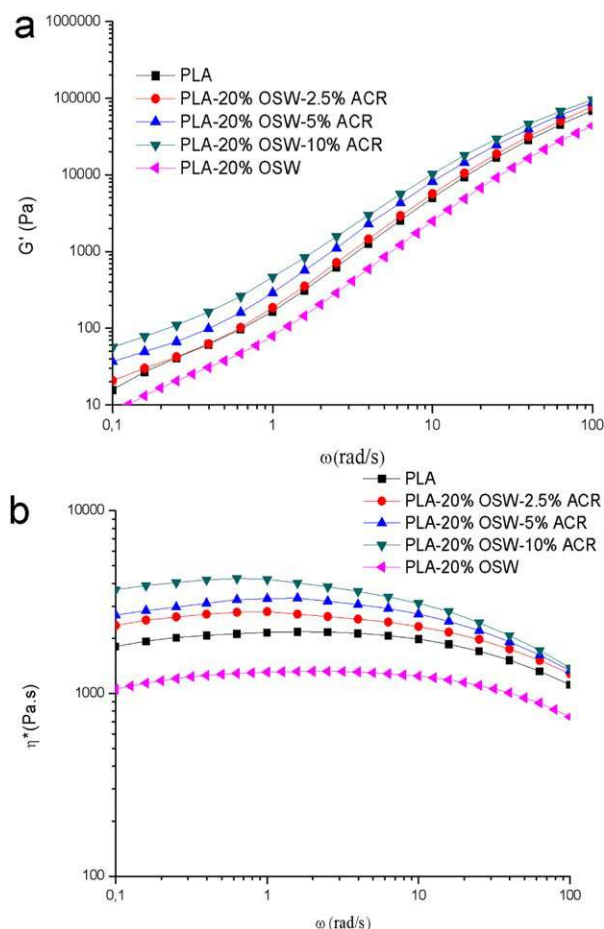


FIG. 4. Evolution of the dynamic complex viscosity (a) and storage modulus (b) versus angular frequency for neat extruded PLA and PLA/OSW (80/20) biocomposites with different ACR amounts at $T = 180^{\circ}\text{C}$. [Color figure can be viewed at wileyonlinelibrary.com]

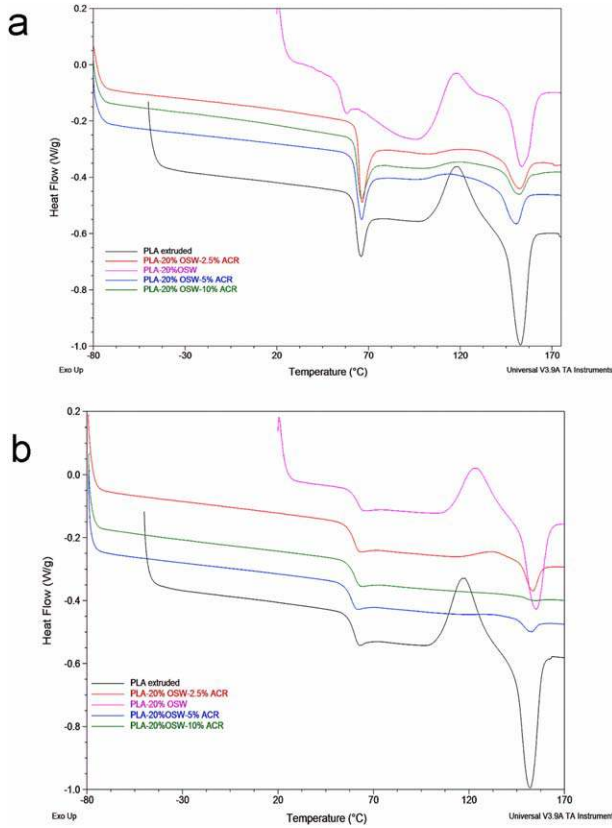


FIG. 5. DSC thermograms obtained upon the first (a) and the second (b) heating scan for neat PLA and PLA/OSW (80/20) biocomposites with different ACR contents. [Color figure can be viewed at wileyonlinelibrary.com]

the interactive forces developed at this level strengthened linkages between the phases (matrix and dispersed CS).

The variation in storage modulus as a function of frequency is shown in Fig. 4b. The storage modulus of the biocomposite without ACR was lower than that of the neat extruded PLA. This can obviously be explained by the PLA degradation process in the presence of OSW [15]. However, the incorporation of ACR into the PLA/OSW biocomposites significantly raised the elastic modulus G' when increasing the CS (ACR) amount. Indeed, at low angular frequencies, the PLA–20% OSW biocomposite exhibited a modulus of about 10 Pa while the biocomposite containing 10 wt% ACR presented a value of around 100 Pa. This was a consequence of the physical network effect created at the contact area between the phases, thereby inducing the formation of an interphase which would consolidate the composite system structure. The material's elastic modulus in the molten state was thus greatly enhanced [31].

It is worth mentioning that for the biocomposites comprising 2.5 wt% ACR, the storage modulus increase was not significant. These biocomposites exhibit almost the same G' values as the neat PLA, but a higher viscosity modulus than the pure PLA. An increase in the viscosity modulus is due to both elastic and viscous contribution. For the last one, the hydrodynamic interactions, the OSW–OSW, ACR–ACR interactions, and the polymer chains between them, affect the measured viscosity. In fact, the composites viscosities at a specific angular frequency can be calculated through shifting the matrix viscosity by a function $\psi(\phi)$ as shown in the following equation:

$$\text{Eta} \times (\phi, \omega) = \text{Eta} \times (0, \omega) \times \psi(\phi). \quad (2)$$

where ω and ϕ are, respectively, the angular frequency and volumetric fraction of the filler, $\psi(\phi)$ is a function that represents the hydrodynamic interactions.

G' should be sensitive if there is some network or high chains entanglement in the suspension. Meanwhile, this result might be also due to the competition occurring between the antagonistic effects of the hydrophilic filler and the core–shell particles. In fact, the presence of the OSW filler causes the degradation mechanism of the PLA matrix whereas the ACR particles enhance the melt elasticity. At a low ACR content (2.5 wt%), the degradation effect dominated the anchoring effect, thus giving rise to a decreased storage modulus.

In the high frequencies range, $G'(\omega)$ converged to a plateau with an invariable amplitude regardless of the content of CS particles. Hence, the flow became independent of the weight percentage of ACR present in the system. This could be explained as follows: At the low frequencies range, the oscillation times are long. It would therefore be possible to probe the entangled and long chains. However, at high frequencies, the measured times are short in comparison with the longer relaxation times and involve only the small chains with low molar masses.

Thermal Properties

Before Annealing. Figure 5 displays the obtained thermograms of the first (a) and second (b) heating scans for neat PLA and the biocomposites containing various CS contents. The thermal characteristics are reported in Table 2 in terms of glass transition temperature (T_g), cold crystallization temperature (T_{cc}), cold crystallization enthalpy (ΔH_{cc}), melting temperature (T_m), and melting enthalpy (ΔH_m). T_{cc} , ΔH_{cc} , T_m , and ΔH_m were determined from the first heating scan since upon the second one the cold crystallization and the melting phenomena disappeared for the systems incorporating CS particles, causing the material to become amorphous. However, the glass transition temperatures

TABLE 2. Thermal characteristics of neat PLA and PLA/OSW (80/20) composite containing various ACR rates.

Samples	Glass transition		Cold crystallization		Melting		Crystallinity
	T_g (°C)	T_{cc} (°C)	ΔH_{cc} (J/g)	T_m (°C)	ΔH_m (J/g)	ζ_c (%)	
PLA extruded	57.5	117	19.9	152	23.4	3.8	
PLA–20% OSW	58.3	116	8.2	153.5	18	13.2	
PLA–20% OSW–2.5% ACR	56.4	121	3.9	152	5.4	4	
PLA–20% OSW–5% ACR	55	123	2.4	150.8	5.3	2	
PLA–20% OSW–10% ACR	56.8	124	3.7	151	4.2	1	

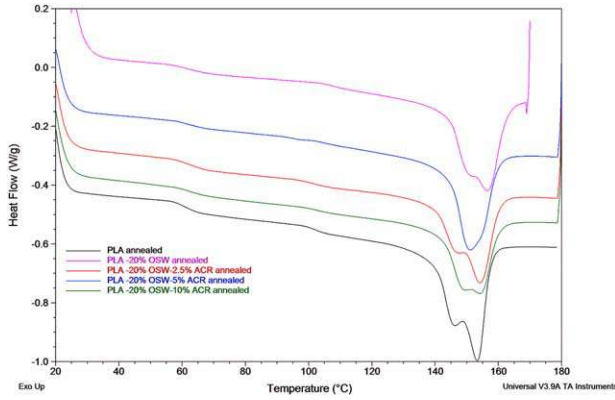


FIG. 6. DSC thermograms obtained upon the first heating scan for annealed PLA and annealed biocomposites PLA/OSW (80/20) with different ACR contents. [Color figure can be viewed at wileyonlinelibrary.com]

(T_g) were assessed from the second heating scan, considering that during the first one, an endothermic peak related to the physical aging of the material was visible near T_g thus hindering an accurate determination of the latter.

For all the samples, the cooling ramp conducted at $10^\circ\text{C}/\text{min}$ from 170°C down to -80°C did not divulge any crystallization peak. This was attributed to the low crystallization rate of the PLA polymer. Several previous studies have confirmed the slow crystallization kinetics of PLA [32, 33].

The thermograms of the biocomposites comprising different CS contents showed a single T_g suggesting a possible miscibility between the PMMA of the CS and PLA. The presence of CS particles in the biocomposite had no significant influence on the glass transition temperature but caused a slight decrease in melting temperature. Furthermore, the CS particles induced a rise of the cold crystallization temperature. As for the cold crystallization peak, it became almost invisible. These results suggest that the PLA crystallization became more difficult in the presence of CS particles. In fact, the entanglements established between PLA chains and amorphous PMMA chains located on the periphery of the CS, restricted the mobility of the macromolecules. Therefore, in addition to its low crystallization kinetics, PLA was further constrained and could not perform any reorganization to form crystals.

As shown in Table 2, the crystallinity level (χ_c) of the composites decreased when increasing the percentage of CS particles dispersed in the system. These results indicate that the presence of ACR diminished the segmental mobility of the PLA molecular chains, causing a reduction in its melting temperature and severely restricting its ability to crystallize during the melt processing.

After Annealing. After extrusion, the PLA/OSW biocomposites were rapidly quenched to room temperature, causing the polymer chains to freeze thus drastically reducing their segmental mobility. However, such an annealing treatment was able to promote the rearrangement process of the PLA molecular chains. Following the annealing, analyses were performed in order to determine associated molecular reorganization phenomena affecting the crystallization and the melting mechanisms of the biocomposites with different CS amounts. The DSC thermograms collected during the first heating are illustrated in Fig. 6.

For all the samples, the peak relative to the glass transition of the PLA component disappeared. Since the annealing temperature (90°C) was higher than the glass transition temperature (57°C), the rate of the amorphous phase was greatly reduced during the annealing treatment. Accordingly, the T_g could not be detected by DSC.

It is worth noting that not all compositions presented a cold crystallization peak. Indeed, since the annealing treatment was conducted at a temperature above T_g , the segmental mobility was great enough to generate densely ordered domains [34]. In addition, the time (3 h) was sufficiently long to permit a segmental rearrangement. In other words, the disordered conformation could easily develop into an ordered phase.

As shown in Fig. 6, all the studied compositions exhibited a double melting peak. A first peak (T_{m1}) between 146 and 152°C , and a second one (T_{m2}) between 153 and 157°C , were detected. This duplication of the endothermic melting peak can be explained by the melt-crystallization phenomenon of the material [35]. In fact, when the crystallization occurs at low temperature and/or high rate, small crystals or defective crystals develop in the material. Upon melting, these crystals are the first to melt at a temperature below the thermodynamic melting temperature. This helps them crystallize into more perfect crystals whose melting will take place at a higher temperature. The resultant endothermic peak that was observed was thus a superposition of two endotherms and an exotherm. The absence of the exotherm indicates that the recrystallization was only partial.

The PLA crystallinity percentages (χ_c) calculated from the DSC results are presented in Table 3. As mentioned previously, the different formulations were quickly quenched after extruding from the melting stage, a fact that made the polymer chains freeze and led to an extremely low χ_c . The annealing heat treatment carried out at a temperature higher than T_g implied a substantial increase in χ_c . This was attributed to an improved mobility of the molecular chains resulting in a certain ease of orientation. Consequently, the rearrangement of the molecular chains into a crystal lattice was favored.

TABLE 3. Thermal characteristics obtained after annealing neat PLA and PLA/OSW (80/20) composite containing various ACR rates.

Samples	Melting		ΔH_m (J/g)	Percent crystallinity χ_c (%)
	T_m ($^\circ\text{C}$)			
	T_{m1}	T_{m2}		
PLA-20% OSW annealed	151.2	156.6	23.4	31.4
PLA-20% OSW-2.5% ACR annealed	146.6	154.2	22.3	30.9
PLA-20% OSW-5% ACR annealed	151	154	24	33
PLA-20% OSW-10% ACR annealed	149.2	154.3	20.5	31.5

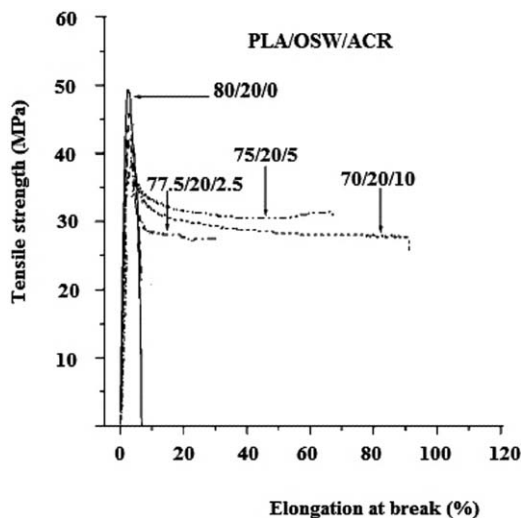


FIG. 7. Tensile behavior of PLA/OSW biocomposites containing 20 wt% of OSW and various acrylic copolymer ratios (0, 2.5, 5, and 10 wt%).

Mechanical Properties

Figure 7 shows the tensile strength variation as a function of the elongation at break, and the results from the tensile and impact tests are summarized in Table 4, in terms of Young's modulus, tensile strength, elongation at break and impact strength. As can be seen in Fig. 7, the inclusion of the acrylic copolymer particles caused significant changes in the tensile behavior of the PLA/OSW biocomposites. Thus, it is worth mentioning that within the elastic range, the material became softer through the deformation resistance reduction, depending on the content of CS particles in the composite (Table 4).

Therefore, the stress propagating through the matrix until the dispersed CS nodules were reached would be supported by the elastomeric component of the CS phase, which has a considerable facility for deformation. Accordingly, an obvious decline in Young's modulus can be noted. This assumes a good adhesion at the contact of PLA-CS components, through the establishment of an interphase which was induced by the proven miscibility between the PLA and PMMA polymers. Hence, the stress would be easily transmitted from the matrix to the CS particles which participated in the consumption of energy necessary for the deformation of the whole system. In other words, the CS particles imparted an improved flexibility to the material.

Moreover, in the break zone, the tensile strength of the PLA/OSW composite was 55 MPa, while the elongation at break was only 3.6%, which means that the material showed a brittle tensile behavior. Nevertheless, all the other compositions

containing CS particles of the acrylic copolymer exhibited a ductile behavior, given the observed increase in elongation at break which reached 91% for the sample comprising 10 wt% of ACR. Beyond the elastic limit, the deformation continued to expand while the stress remained almost constant and the systems broke with a high elongation as compared to the composite without ACR. The tensile strength did not show a substantial decrease; it remained rather high for the formulations with different CS contents. The recorded minimum value was 36 MPa for the system comprising 10 wt% of ACR (Table 4).

The impact strength was measured for the biocomposites processed with different amounts of acrylic additive, and the results are given in Table 4. The impact strength value drastically increased from 1.2 kJ/m² for the PLA/OSW (80/20) biocomposites to 103 kJ/m² for the biocomposite including 10 wt% of the acrylic copolymer. In fact, the density of entanglements established at the interface between PMMA and PLA increased with the ACR content. This induced a rise of interactive forces at the contact area between the PLA matrix and the CS particles [22]. The compatibility between PLA and a core-shell type acrylate copolymer has been reported by some authors [23]. Thus, the elastomer settled in the central nucleus of the CS particle was deemed responsible for the observed improvement of both elongation at break and impact strength of the biocomposites, due to the greater ability to absorb the required energy to break the sample.

Morphological Study

Given the complex structure of the studied systems, the morphology of the PLA/ACR blends (without addition of OSW) was first explored in order to assess the interface quality and the dispersion uniformity of CS particles in the PLA matrix. Figure 8 illustrates the SEM micrographs of the fractured surfaces of the PLA/ACR blends at the compositions of (95/5) and (90/10). A nodular morphology, with the nanometric core-shell particles (with a dimension of about 300 nm) dispersed in the PLA continuous phase, can be observed. The spherical CS particles seemed to be quite distinct from the matrix and exhibited a homogenous distribution. They were embedded in the structure and did not contain any voids at their peripheries. Besides, the absence of empty cavities substantiated the fact that the CS particles were not pulled out from the matrix upon fracture, but remain anchored in the matrix. The adhesion at the boundaries of the component appeared to be quite adequate. This reflects a perfect miscibility between the PLA matrix and glassy PMMA shell, which resulted in the formation of a thin interphase layer distributed around the dispersed CS particles. In fact, according

TABLE 4. Mechanical properties of neat PLA and PLA/OSW (80/20) biocomposites without and with core-shell-type acrylic copolymer.

PLA/OSW/ACR	Young's modulus, E (MPa)	Elongation at break (%)	Tensile strength (MPa)	Impact strength (kJ/m ²)
100/0/0	2,060 ± 23	6 ± 0.5	60 ± 2	2.6 ± 1
80/20/0	1,888 ± 25	3.6 ± 0.6	53 ± 3	1.2 ± 0.5
77.5/20/2.5	1,510 ± 20	30 ± 7	45 ± 1.2	8 ± 3
75/20/5	1,370 ± 40	67 ± 5	44 ± 1.3	45 ± 5
70/20/10	1,120 ± 25	91 ± 9	36 ± 1	103 ± 7

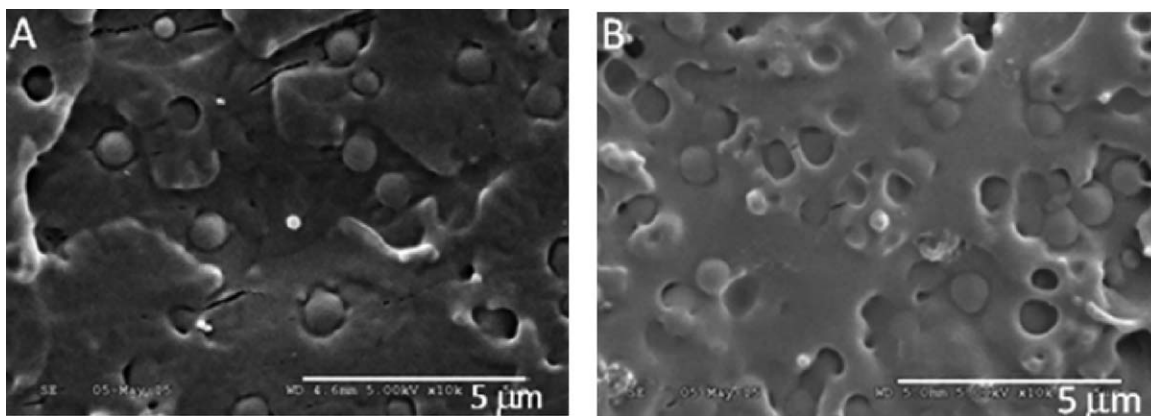


FIG. 8. Micrographs of PLA/ACR blends (a) 95/5 and (b) 90/10.

to the micrographs of the PLA/ACR blends, especially for the (90/10) composition, the dispersed core-shell nanoparticles seemed to be coated with a film corresponding to the interphase in which the miscible polymers PLA and PMMA coexisted.

As can be seen in Fig. 9, the morphology of the fractured surface of the PLA/OSW composite (Fig. 9a) was markedly different from that of the biocomposite processed with 10 wt% of CS particles. When ACR was added to the PLA/OSW (80/20) biocomposite, the OSW microparticles became well maintained in the structure (Fig. 9b). In addition, the voids at the interface were clearly reduced and a certain structural continuity was established by coating the OSW particles with a thin layer of PMMA. The latter seemed to be more interactive with the OSW particles than its PLA counterpart. Thereafter, the adhesion at the PLA-OSW interface would be greatly improved and the cohesion of all the composite system components (OSW, PLA, and core-shell) would become ostensibly consolidated.

While the functional ester groups of PLA are situated at the chain trunk, those of PMMA are in the form of groups along the chain. They were thus more unhindered and exhibited a better ability to interact with the OSW particles. As they settled on the surface of the OSW particles, they covered them with a polymer film.

CONCLUSIONS

In order to investigate the effect of acrylic core-shell particles on the thermal, rheological and mechanical properties of PLA/OSW biocomposites, different PLA/OSW/ACR formulations were prepared by twin screw extrusion. The study of solid-state viscoelastic properties revealed that the addition of core-shell particles conferred an improved flexibility to the biocomposites.

The thermal analyses showed miscibility between PLA and the shell of the acrylic additive: a single T_g was observed. The cold crystallization temperature increased and the crystallinity rate decreased with the increasing ACR content, indicating that the core-shell particles restricted the ability of the PLA chains to crystallize and/or recrystallize during the melt processing.

The dynamic rheological tests in the molten state divulged a significant increase in complex dynamic viscosity and elastic modulus with an increasing amount of CS. These findings suggest the creation of entanglements between the PLA chains and those of PMMA on the surface of the dispersed CS particles. The physical network, thus generated, reduced the PLA segmental mobility and enhanced the melt elasticity.

The mechanical study demonstrated an improvement of both elongation at break and impact strength, and the morphological observations corroborated the obtained results. In fact, an

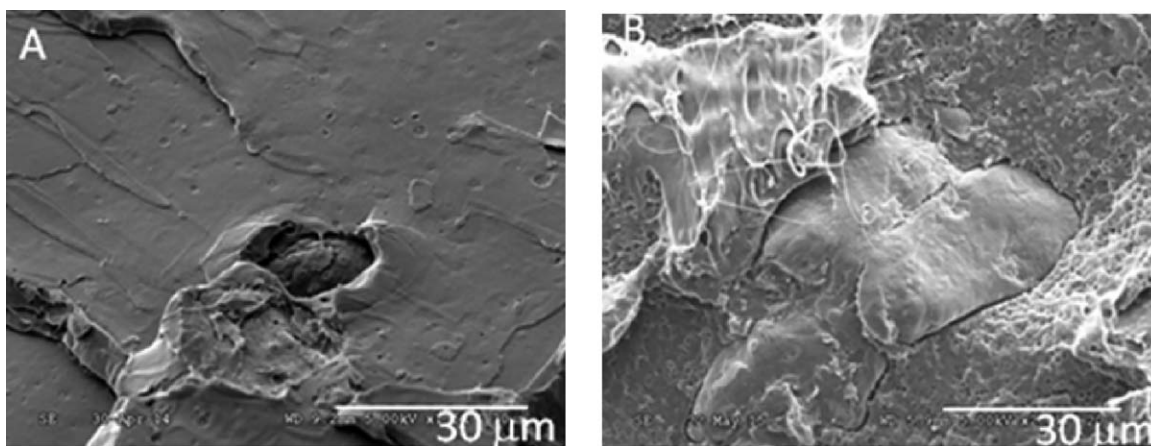


FIG. 9. Micrographs of PLA/OSW (80/20) biocomposites without (a) and with (b) 10 wt% of acrylic additive.

obvious enhancement of the adhesion between the components was noted for PLA–CS as well as PLA–OSW.

REFERENCES

1. S. Kalia, B.S. Kaith, and I. Kaur, *Polym. Eng. Sci.*, **49**, 1253 (2009).
2. J.P. López, S. Boufi, N.E. Mansouri, P. Mutjé, and F. Vilaseca, *Compos. B: Eng.*, **43**, 3453 (2012).
3. A.I. Krishnan and J.M. Torkelson, *Polym. Compos.*, **34**, 1211 (2013).
4. J.K. Pandey, S.H. Ahn, C.S. Lee, A.K. Mohanty, and M. Misra, *Macromol. Mater. Eng.*, **295**, 975 (2010).
5. A. Ashori, *Bioresour. Technol.*, **99**, 4661 (2008).
6. M. Khemakhem, K. Lamnawar, A. Maazouz, and M. Jaziri, *Polym. Eng. Sci.*, **56**, 27 (2016).
7. F. Achmad, K. Yamane, S. Quan, and T. Kokugan, *Chem. Eng. J.*, **151**, 342 (2009).
8. S. Anders and S. Mikael, *Prog. Polym. Sci.*, **27**, 1123 (2002).
9. K. Van de Velde and P. Kiekens, *Polym. Test.*, **21**, 442 (2002).
10. K.M. Nampoothiri, N.R. Nair, and R.P. John, *Bioresour. Technol.*, **101**, 8493 (2010).
11. Y. Fan, H. Nishida, Y. Shirai, Y. Tokiwa, and T. Endo, *Polym. Degrad. Stab.*, **86**, 197 (2004).
12. S.A. Kelly, M.S. Kathleen, and A.H. Marc, *Polym. Rev.*, **48**, 85 (2008).
13. H.Z. Liu and J.W. Zhang, *J. Polym. Sci. B: Polym. Phys.*, **49**, 1051 (2011).
14. Z. Kulinski and E. Piorkowska, *Polym. J.*, **46**, 10290 (2005).
15. M. Khemakhem, K. Lamnawar, A. Maazouz, and M. Jaziri, *Polym. Compos.* (2016). doi:10.1002/pc.24094.
16. D. Olmos, R. Vela, A. Alvarez-Junceda, and J. Gonzalez-Benito, *J. Adhes.*, **89**, 697 (2013).
17. M. Pan, L. Zhang, J. Yuan, and X. Wang, *Acta Polym. Sin.*, **1**, 47 (2005).
18. D.X. Zha, Y.F. Yao, and X.J. Cao, *J. Zhejiang Sci. Tech. University*, **29**, 812 (2012).
19. H. Zhang, N. Liu, X. Ran, C. Han, L. Han, Y. Zhuang, and L. Dong, *J. Appl. Polym. Sci.*, **125**, E550 (2012).
20. S.L. Sun, M.Y. Zhang, H.X. Zhang, X.M. Zhang, and X.M. J. *Appl. Polym. Sci.*, **122**, 2992 (2011).
21. Y. Hao, H. Liang, J. Bian, S. Sun, H. Zhang, and L. Dong, *Polym. Int.*, **63**, 660 (2014).
22. N. Wu, M. Ding, J. Zhang, and R. Lin, *Mater. Lett.*, **83**, 148 (2012).
23. T. Li and L.S. Turng, *Polym. Eng. Sci.*, **46**, 1419 (2006).
24. G. Zhang, J. Zhang, S. Wang, and D. Shen, *J. Polym. Sci. B: Polym. Phys.*, **41**, 23 (2003).
25. W. Li, D. Wu, S. Sun, G. Wu, H. Zhang, Y. Deng, H. Zhang, and L. Dong, *Polym. Bull.*, **71**, 2881 (2014).
26. B. Meng, B. J. Deng, Q. Liu, Z. Wu, and W. Yang, *Eur. Polym. J.*, **48**, 127 (2012).
27. X.G. Ge, S. George, S. Law, and M. Sain, *J. Macromol. Sci. Phys.*, **50**, 2070 (2011).
28. T. Murayama, *Dynamic Mechanical Analysis of Polymeric Material*, Elsevier Scientific Pub. Co, Netherlands (1978).
29. H. Liang, Y. Hao, J. Bian, H. Zhang, L. Dong, and H. Zhang, *Polym. Eng. Sci.*, **55**, 386 (2015).
30. X. Hao, J. Kaschta, X. Liu, Y. Pan, Y. and D.W. Schubert, *Polymer*, **80**, 38 (2015).
31. M. Hernández-Alamilla, and A. Valadez-Gonzalez, *J. Polym. Eng.*, **36**, 31 (2016).
32. J.T. Yeh, J.T. C.H. Tsou, C.Y. Huang, K.N. Chen, C.S. Wu, and W.L. Chai, *J. Appl. Polym. Sci.*, **116**, 680 (2010).
33. S. Saeidlou, S. M.A. Huneault, H. Li, and C.B. Park, *Prog. Polym. Sci.*, **37**, 1657 (2012).
34. S. Lv, J. Gu, J. Cao, H. Tan, and Y. Zhang, *Int. J. Biol. Macromol.*, **74**, 297 (2015).
35. D.J. Blundell, *Polymer*, **28**, 2248 (1987).